Assessing Indoor Hygrothermal Conditions in Unfavourable Scenarios: Open Windows in a Residential Building in the Coastal Mediterranean Summer Climate

Daniel Antón *

a) Departamento de Expresión Gráfica e Ingeniería en la Edificación, Escuela Técnica Superior de Ingeniería de Edificación, Universidad de Sevilla, Seville 41012, Spain
b) Product Innovation Centre & The Creative and Virtual Technologies Research Lab, School of Architecture, Design and the Built Environment, Nottingham Trent University, Nottingham NG1 4FQ, UK

*Corresponding author

Amin Al-Habaibeh

Department of Product Design, School of Architecture, Design and the Built Environment, Nottingham Trent University, Nottingham NG1 4FQ, UK

Manuel J. Carretero-Ayuso

Department of Architectural Graphic Expression, Higher Polytechnic School, University of Extremadura, Cáceres 10003, Spain

Madelyn Marrero

Departamento de Construcciones Arquitectónicas II, Escuela Técnica Superior de Ingeniería de Edificación, Universidad de Sevilla, Seville 41012, Spain

Abstract

Scientific research has identified different adaptive behaviours that influence thermal comfort in buildings. Depending on factors such as ventilation mode, building type, or occupant age, those user actions are diverse and include air conditioning and fan usage, window and/or door opening, curtain and/or blind usage, cloth adjustment, and beverage drinking, among many others. Especially in the Mediterranean summer climate, façade openings are likely to be a direct inflow of hot air. Focusing on the case study of a residential building with a robust envelope, this chapter aims to assess the impact of keeping windows open on indoor temperature and relative humidity.

Keywords: Open windows; Mediterranean climate; Summer climate; Temperature; Relative humidity.

1. Introduction

Scientific research has identified different adaptive behaviours that influence thermal comfort in buildings. Depending on factors such as ventilation mode, building type, or occupant age, those user actions are diverse and include air conditioning and fan usage, window and/or door opening, curtain and/or blind usage, cloth adjustment, and beverage drinking, among many others (Arsad et al. 2023).

Despite the multifaceted nature of adaptive strategies, research has predominantly concentrated on a limited set of passive measures, such as optimising insulation layers, utilising naturally ventilated envelopes, and employing sun shading devices (Balali et al. 2023). Often driven by considerations of energy efficiency and financial implications, these adaptive strategies point out the need for a more comprehensive exploration of alternative approaches.

Chvatal and Corvacho (2009) delved into the impact of increased envelope insulation on overall building performance, revealing its beneficial effects during winter but raising concerns about potential overheating in summer. Given the conventional perception of highly insulated envelopes as unequivocal energy-saving solutions, it is therefore necessary to determine optimal insulation levels to avoid both indoor hygrothermal discomfort and increased reliance on air conditioning.

Understanding the influence of outdoor environmental parameters on window-opening behaviour, Kim et al. (2019) provided valuable insights for informed design decisions in architecture. According to Mochida et al. (2005), cross-ventilation emerges as a key factor and has the potential to significantly enhance indoor thermal comfort, especially in the summer, through strategic control of window openings and tree arrangements. Likewise, Daghigh (2015) drew attention to the impact of natural ventilation on indoor humidity and its impact on comfort.

Additionally, Tamaskani Esfahankalateh et al. (2021) highlighted the significance of window orientation for enhancing thermal comfort in residential buildings, recommending east- and west-facing openings for cold climates. The authors also indicated that heat transfer between the body and the surrounding environment happens through convection, so wind speed turns out to be relevant in this sense.

Li et al. (2015) explored the triggers for window opening, emphasising the role of outdoor air temperature and occupants' desire to improve indoor thermal and air quality against outdoor relative humidity, indoor air temperature, indoor relative humidity, and indoor CO_2 concentration.

Further nuances in window-opening patterns were exposed in a year-long study by Lai et al. (2018), demonstrating variations across seasons, times of day, and weekdays against weekends. It is worth noting that, in the region of their study (China), opening patterns increased from winter to summer up to around 27°C, with greater activity during the morning and working hours on weekdays; window opening on weekends took place to a lesser extent.

The diverse perspectives presented in the literature stress the complexity of adaptive behaviours influencing thermal comfort in buildings. Especially in the Mediterranean summer climate, façade openings are likely to be a direct inflow of hot air and entail a temperature increase, especially in south rooms. According to Zaki et al. (2012), occupants may depend on mechanical cooling to counteract the excessive solar gain of rooms, which causes thermal discomfort. In this line, focusing on the case study of a residential building with a robust envelope, this chapter aims to evaluate how keeping windows open affects indoor temperature and relative humidity based on sensor and satellite data collected during a specific two-week period in summertime. Further, this unfavourable scenario was exacerbated by wildfire activity in the immediate vicinity, substantially reducing the area's humidity during that period and for the foreseeable future, thus making it necessary to picture the relative humidity of the case study area. After all, in addition to indoor hygrothermal conditions, thermal comfort is affected by people's adaptation to climate, of which the role of relative humidity is more complex (Borghero et al. 2023).

Having introduced the research context, this chapter is structured as follows: Section 2 describes the case study and its geographical context. Meanwhile, Section 3 presents the research methodology, which is supported by own and third-party data on the case study building and its surroundings. Section 4 presents the data achieved and discusses the findings. Finally, Section 5 gathers the drawn conclusions and future work.

2. Case study: a residential building with a robust envelope

2.1. Context

As seen in Fig. 1 and Fig. 2, the case study is located in Alhaurín de la Torre, the 7th most populated municipality in the near vicinity of Málaga city (42,531 citizens in 2022, according to data by the regional government's Instituto de Estadística y Cartografía de Andalucía in 2023). Geographically speaking, the case study is on the north side of Sierra de Mijas and close to the Guadalhorce River valley and coastal villages. The building is specifically located in Pinos de Alhaurín, a leafy suburb, at approximately 245 metres above sea level, near a calcite quarry and a pine forest.

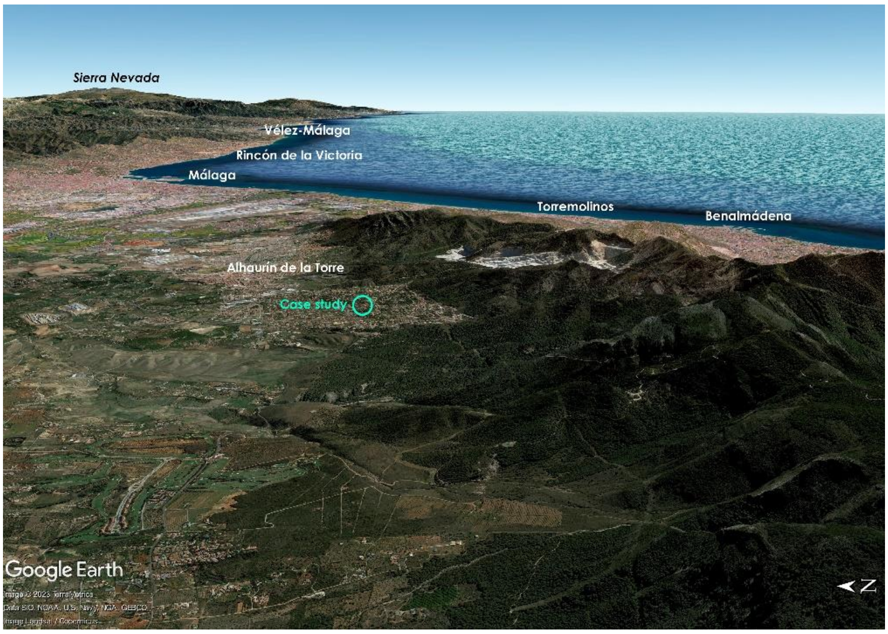

Fig. 1. Case study's geographical context: Sierra de Mijas and coastal surroundings. Viewed from the west. Source: based on Google Earth Pro 3D content (Google Inc. 2023).

Fig. 2. Case study's geographical context: Sierra de Mijas and coastal surroundings. Viewed from the northeast. Source: based on Google Earth Pro 3D content (Google Inc. 2023).

The Sierra de Mijas is a mountainous formation with a variety of flora and fauna, highlighting the presence of the Jarapalos Arboretum, a botanical garden with a multitude of plant species. Unfortunately, these mountains are prone to wildfires (mainly intentioned), especially in summer. In this sense, from 12.30 pm on the 15^{th} to 17^{th} (stabilised at 7.30 pm) of July 2022, the Sierra de Mijas experienced a devastating wildfire affecting biodiversity. It was not until 19^{th} July that the fire was controlled and finally declared extinguished on 3^{rd} August 2022. It is also worth mentioning that authorities evacuated more than 1500 people preventively since the fire reached, and was likely to reach, populated areas. In relation to the extent (in hectares burnt) of this natural disaster, official numbers differ depending on the reporting public body or organisation: 1788.33 ha (Dirección General de Protección Civil y Emergencias 2023), approximately 1870 ha by the regional government (Dirección General de Política Forestal y Biodiversidad 2023), or 1814.05 ha measured on cartography and 2097.21 ha calculated on the Digital Terrain Model (DTM) of the area a few hours before the fire was stabilised in the evening (Acaire 2022). Fig. 3 shows, in red colour, the surface boundary affected by the wildfire, according to Sentinel 2B satellite data at 10.56 am on 17^{th} July.

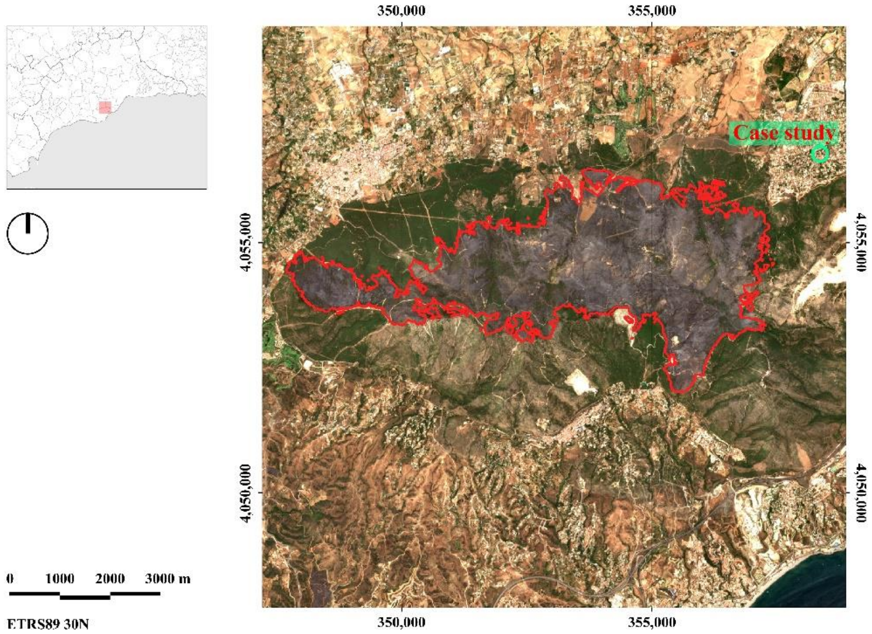

Fig. 3. Location and extent of Sierra de Mijas' wildfire on 17th July 2022. Source: based on Javier Martos' map (Acaire 2022).

Section 4 will reveal the role of this foliage-covered sierra in the area's moisture, but now that it has been almost destroyed, the climatic implications of this wildfire are yet to be determined.

2.2. Building typology and features

The construction of the case study building concluded in 1999, several years before the entry into force of the continuously amended and current Technical Building Code (Ministerio de Vivienda 2006), the reference set of regulations that establish the requirements and standards for building design and construction in Spain. Notwithstanding, despite the regulations applicable to date (1970s to 1980s), the building was provided with a robust envelope with thermal insulation and a significant mass in walls, thus yielding a reasonable theoretical thermal inertia.

The case study's building was a ground-floor detached house with a reinforced concrete structure based on pillars and slabs and a sloping roof. The walls forming the thermal envelope were 34.5 cm thick and consisted of the following layers, from the outside to the inside: First, white vibrated concrete rough blocks (there was no additional cladding), a 2 cm layer of cement mortar to seal the blocks and receive the projection of 2 cm of polyurethane foam. Next, letting a non-ventilated 3 cm cavity in the inner core of the wall to reduce thermal transmittance, a hollowbrick wall with a thickness of 7 cm served as the basis of the 1.5 cm thick plastering in contact with indoor ambient.

The two monitored rooms of the building had different orientations at opposite façades, particularly south and north. Each room comprised one sliding window with an effective opening surface of approximately 0.50 m^2 (0.45 x 1.10 m) for each open sash. These windows allowed cross-ventilation throughout a corridor.

3. Methodology

The research methodology comprises two different data sources: 1) Satellite imagery and data, and 2) Data recorded in situ from the case study building.

3.1. Satellite data collection

3.1.1. Satellite imagery

Sentinel-2 L2A data were used to contextualise the case study in terms of geomorphological features, its proximity to the sea, and the surrounding dryness in order to supplement recorded hygrothermal data from the case study building.

Access to satellite data was granted via the Copernicus Browser from the Copernicus Data Space Ecosystem (European Space Agency (ESA) and T-Systems 2017). According to this online system, Sentinel-2 satellite provides high-resolution visible and infrared spectral band images to monitor vegetation, soil and water cover, inland waterways, and coastal areas to achieve land-cover maps, land-change detection maps, vegetation monitoring, or monitoring of burnt areas. Level 2A data, available since June 2015 and March 2017 globally, are high-quality data processed to filter atmospheric effects on the light reflected off the Earth's surface, reaching the sensor.

Collected satellite imagery comprised two distinct types:

- 'True colour' images (visible light) consisting of the red, green, and blue (RGB) colour channels to produce a natural coloured representation of the Earth, as seen with the naked eye.
- 'Normalised Difference Moisture Index' (NDMI) images, with values ranging from -1 to 1 (coefficient). Low, negative values (intense red) indicate barren soil, values around zero (from approximately -0.2 to circa 0.4) generally correspond to water stress, and high, positive values (dark blue) account for high canopy with no water stress. In this way, NDMI images are used to determine vegetation water content and monitor droughts.

The time span of satellite image recording was determined by the following factors: i) the hygrothermal monitoring period of the case study building, so that it was mostly covered (from 9th to 23rd July 2022), ii) the wildfire that took place nearby during that period, and iii) the comprehensiveness and quality of satellite imagery. The second factor made it convenient to explore the area's moisture conditions before and after the natural disaster, which happened from noon on the 15th until the evening of the 17th of July 2022, in order to reveal a possible impact on the indoor and outdoor temperature and relative humidity values of the case study. The latter factor, i.e., the suitability of image data, was affected by the coverage of satellite flight paths over the area and its cloudiness. In an effort to reach the end of the building's monitoring period, satellite imagery was consulted in the days that followed. However, the images were incomplete. It was not until 1st August that the whole area was captured by Sentinel-2 (the moisture conditions may have undergone alterations over that extended time frame) except for 27th July, but the image presented a significant number of clouds covering the Sierra de Mijas. Consequently, it was decided to display 22nd July as the closing instance of the satellite observation. Similarly, pre-wildfire data were retrieved from the Copernicus Browser dated 27th June for comparison, thus ensuring the completeness mentioned above and the quality of image data.

Beyond collecting the satellite images (true colour and NDMI), pre- and post-wildfire histograms were downloaded from the NDMI images so that the moisture index could be more easily visually quantified and understood in terms of significance. In addition, both NDMI images were converted into greyscale to quantify the pixel intensities as per Antón and Amaro-Mellado (2021) and as seen in Antón et al. (2022). This was carried out by enquiring the digital number (DN) in 8-bit encoding (256 values ranging from 0 to 255). As a consequence, the lost vegetation and the new surface with extreme dryness could be represented by means of two supplementary histograms.

3.1.2. Meteorological data

This research also benefitted from meteorological satellite data, which were useful in capturing the outdoor conditions of the case study building's surroundings during indoor hygrothermal monitoring. This was achieved via the POWER Data Access Viewer by NASA (1981) to obtain higher resolution daily time series data from the Prediction of Worldwide Energy Resource (POWER) Project. With its origin in NASA research and managed by NASA's Global Modelling and Assimilation Office (GMAO), POWER provides solar and meteorological data sets to support renewable energy, energy efficiency in buildings, and agricultural needs. Here, meteorological data are provided by the Modern-Era Retrospective analysis for Research and Applications, Version 2 (MERRA-2) Project, available since 1st January 1981, with data until within several months of real time (NASA 2020).

In this research, by entering the case study's coordinates (hidden for privacy), a comprehensive series of meteorological data was extracted from MERRA-2:

- The average air (dry bulb) temperature at 2 metres above the Earth's surface (°C) indicated as T2m in this chapter's tables.
- Dew point (temperature) at 2 metres (°C)
- Relative humidity at 2 metres (%), indicated as RH2m in this chapter's tables.
- Surface pressure (kPa)
- Wind speed at 10 metres (m/s), WS10 in tables
- Wind direction at 10 metres (degrees)
- Wind speed at 50 metres (m/s), WS10 in tables
- Wind direction at 50 metres (degrees)

Among those parameters, the most relevant were chosen to analyse the building performance considering the season of the year, the case study altitude, and prioritising data deriving from the sensors installed.

Finally, the 2022 mean energy intensity or mean solar radiation on the case study area's Earth surface was also obtained to contextualise the case study.

3.2. Sensor data: indoor and outdoor conditions

Data revealing the case study's indoor and outdoor conditions consisted of temperature and relative humidity recordings. This was carried out using three OMEGA data loggers (OM-CP-RHTEMP101A) attached to the walls and configured to monitor strategic case study locations: a bedroom facing the south façade (ID 1_South), a guest room facing north (ID 2_North), and outside the latter room's window, protected from direct sunlight (ID 3_Exterior). It should be noted that both rooms are opposite, thus allowing cross ventilation. Considering that the aim of this research was to ascertain the building's hygrothermal performance, no cooling was used during the monitoring period, letting its passive features be the sole influencing factors.

The temperature and relative humidity monitoring took place every 15 minutes during the 14 days from 9th to 23rd July 2022, commencing and concluding at 12 pm CEST (Central European Summer Time). In the course of that period, records were kept for both instances: i) when windows in any of the rooms were closed and ii) the occupancy status of each room.

After acquiring the data, temperature and relative humidity values were concurrently visualised in individual graphs for each sensor. This presentation aimed to facilitate the comprehension of the relationship between the two variables. Additionally, key statistical parameters, including maximum, minimum, mean, and standard deviation were computed. The analysis approach extended to encompass the coefficient of variation, covariance, and correlation coefficient, contributing to a comprehensive characterisation of their variability and interrelationship.

4. Results and discussion

As per the methodology structure above, this section presents and analyses the data collected by following both qualitative and quantitative statistical approaches.

4.1. Satellite data

4.1.1. Sentinel-2 L2A data

In this research, satellite image data are used to depict the case study area's environmental conditions. In this sense, Fig. 4 shows Sentinel-2 L2A true-colour and NDMI images and histograms before and after the wildfire occurred in Sierra de Mijas. The various data reveal a clear difference between both scenarios, highlighting the significant loss of vegetation towards the barren surface, especially with values ranging from -0.08 to -0.30 in the NDMI images, also seen as forest burnt in the true-colour image. Consequently, as burnt areas retain less moisture than foliage-covered sectors, an impact on the region's climate is expected. In turn, this could impact the hygrothermal conditions of the case study as opposed to the situation in which the wildfire did not occur.

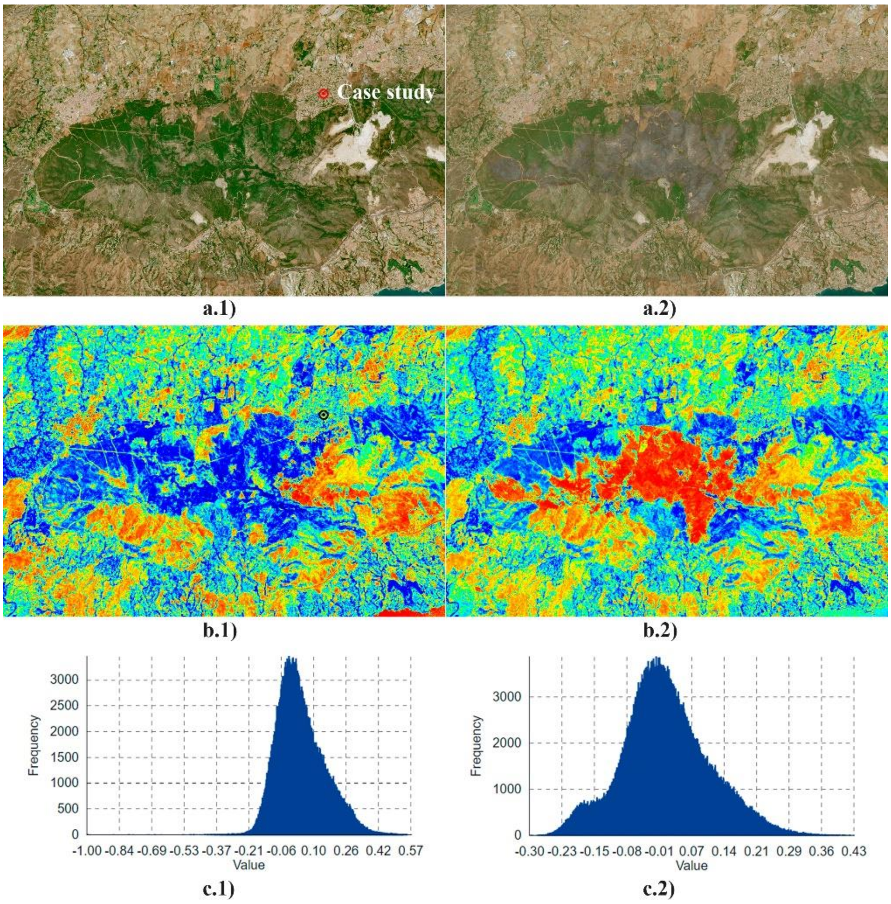

Fig. 4. Sentinel-2 L2A satellite data from Sierra de Mijas' wildfire, pre- (1, left column) and post- (2, right column) wildfire: **a)** true colour images; **b)** NDMI images; and **c)** NDMI histogram. Source: NASA's (1981) 'POWER Project' Data Access Viewer.

In addition, although the conversion of RGB images into greyscale depends on colour interpretation and assignment to index values, pixel intensities were enquired to approximate the quantification of vegetation losses further. The following histograms illustrate the lost vegetation and the new surface with extreme dryness. Thus, based on the converted RGB NDMI images, Fig. 5 quantifies the number of pixels corresponding to this index.

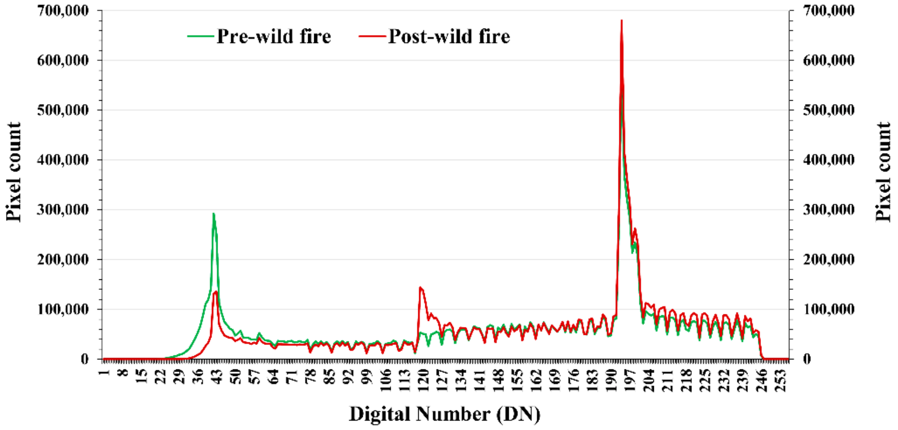

Fig. 5. Histogram of pre- and post-wildfire pixel distribution.

Also shown as the percentage of higher presence (Fig. 6):

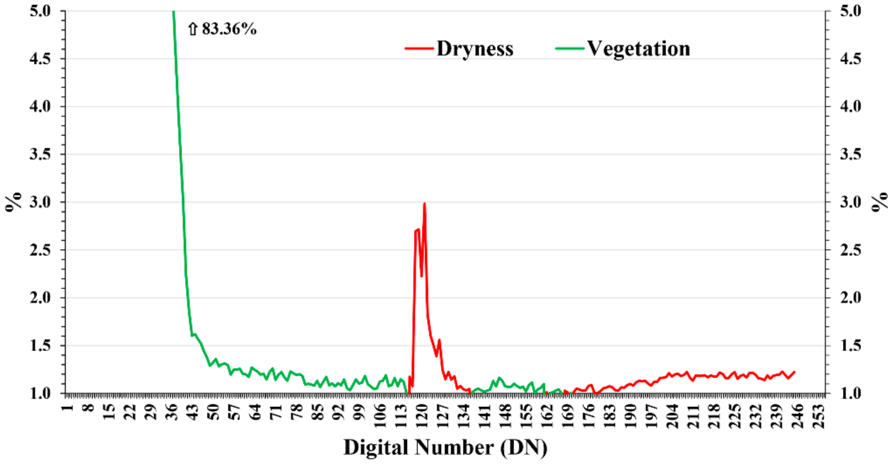

Fig 6. Histogram of vegetation and dryness pixel distribution.

In view of the above, a lower DN represents vegetation, whereas higher DN values account for dry areas, the latter mainly corresponding to burnt surfaces. Thereby, from DN 117 onward, it is the post-wildfire scenario that exhibits a higher presence of pixels corresponding to areas with increased water stress, away from the extremely high percentage of pre-wildfire vegetation from DN 0 to circa 50 and the more slight foliage increase within the 50–117 range.

4.1.2. MERRA-2 meteorological data

Satellite meteorological data collected from NASA's MERRA-2 Project are presented here to determine the quantities applicable to the case study. To do this, these quantities are displayed together by plotting their values throughout the hygrothermal monitoring period set.

Fig. 7 shows MERRA-2 temperature and relative humidity data, which are estimations at 2 m over the Earth's surface. In order to assess their suitability for this study, it is therefore necessary to compare them with outdoor data recorded from the case study building (sensor ID 3_Exterior), although the latter will be addressed in the following subsection.

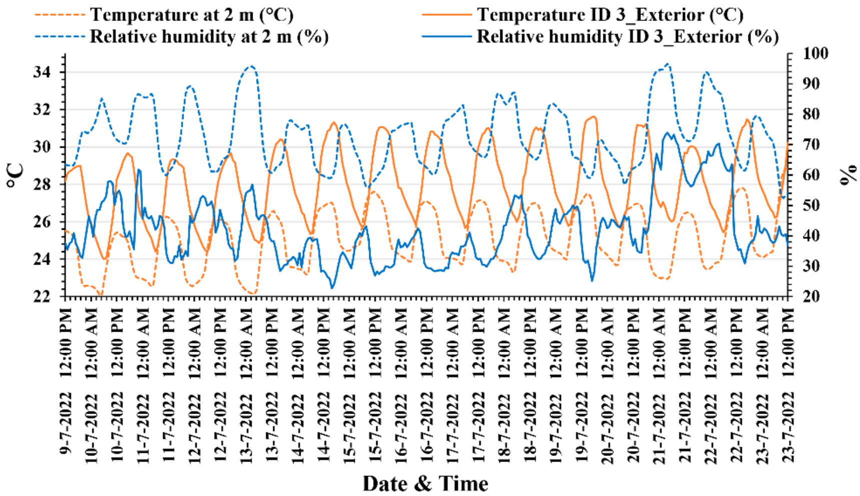

Fig 7. Case study monitoring: outdoor ambient temperature and relative humidity. Source: NASA's (1981) 'POWER Project' Data Access Viewer and sensor ID 3_Exterior, respectively.

To support that decision, quantitative, statistical data from the two-source meteorological parameters above are gathered in Table 1 below:

	Max*	Min*	Mean	Standard Deviation	CoV*	Covariance	Correlation Coefficient
T2m (ºC)	28.83	22.05	25.02	1.56	0.06	1.82	0.61
T Sensor3 (ºC)	31.62	24.00	28.05	1.94	0.07		
RH2m (%)	96.56	52.38	72.97	10.35	0.14	61.89	0.54
RH Sensor3 (%)	73.90	22.70	42.18	11.06	0.26		

*Where 'Max' accounts for maximum, 'Min' for minimum, and 'CoV' for coefficient of variation, and 'T' and 'RH' respectively represent temperature and relative humidity.

Table 1. Statistical analysis of data collected from MERRA-2 and sensor 3.

All considered, both the graph and the analysis results reveal significant differences between data from the two sources, which may lead to wrong insights into the case study's hygrothermal behaviour: MERRA-2's average RH is 73% higher than that deriving from Sensor 3 ID 3_Exterior, while the mean temperature from the former is approximately 11% lower during the monitoring period. Moreover, MERRA-2's temperature rises with sunlight before the actual temperature does, the latter being extracted from Sensor 3's log. This fact is qualitatively shown in the graph above and from the calculated covariance, with a positive relationship revealing a common trend. It is worth noting that negative values indicate an indirect relationship between variables (this is the case of temperature and relative humidity), whereas positive values show that they jointly increase and decrease. Besides, considering their high covariance, the strong direct relationship between relative humidity from the two sources is remarkable since when the recorded RH (sensor) increases, the estimated RH (satellite) rises at a higher rate, which could be away from the ground-floor reality, the case study.

This research did not aim to understand the difference between data from the cited sources (recorded against estimated), but it may be partly due to the fact that the case study presents obstacles to wind, such as the building itself or its surroundings, particularly, a significant number of trees and other nearby constructions.

For all those reasons, it is the temperature and relative humidity recorded by Sensor ID 3_Exterior that is selected to depict the case study's performance.

In addition, Fig. 8 depicts how wind speed at 10 m and 50 m altitude (from the Earth's surface) and surface pressure behaved during the monitoring period.

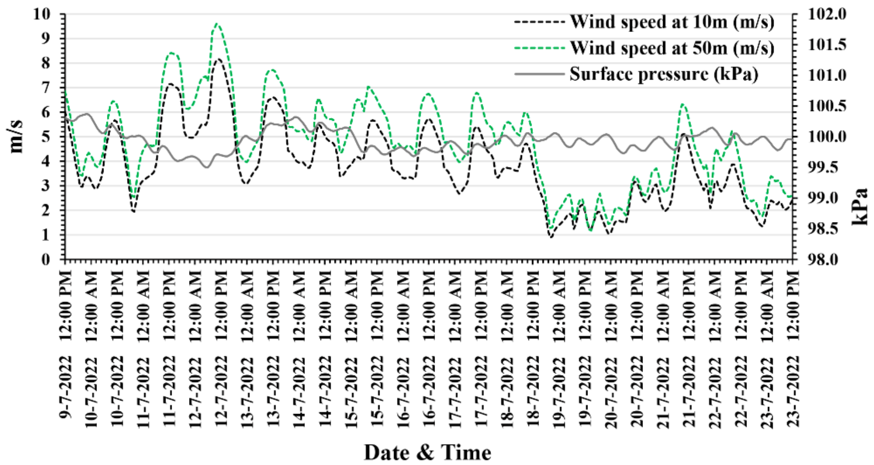

Fig. 8. Case study monitoring: wind speed at 10 m and 50 m, and surface pressure. Source: NASA's (1981) 'POWER Project' Data Access Viewer.

The wind direction at 10 m is not represented in the graph above but follows a quasi-regular behaviour during the monitoring period. However, it was from 8 am on the 19th of July until 12 am on the 20th that the wind experienced a change in direction, progressively blowing from southeast to northwest during that lapse. Given the representation of wind speed in Fig. 8, the clear drop in its values corresponds to the cited change in wind direction, but there is no noticeable impact on the rest of the quantities, at least qualitatively.

Besides, in view of the lower values of wind speed at 10 m in relation to that at 50 m, a reduction in wind speed can be anticipated at a lower altitude (1–2 m against 10 m). As explained above, near the ground level, the building itself and its surroundings constitute obstacles hindering the wind, so this should also have an impact on temperature and relative humidity estimations by MERRA-2. For its part, the dew point (temperature) at 2 m was not analysed, as the recorded (sensor) outdoor temperature was always higher, even at night.

Regarding surface pressure, Fig. 8 above reveals clearly defined rises and falls in cycles of approximately 12 hours each. In light of recorded temperature cycles (of around 24 hours), surface pressure also turns out to be a relevant parameter to study. Therefore, wind speed at 10 m and surface pressure were chosen as the key meteorological (MERRA-2) quantities for the joint analysis with hygrothermal monitoring data.

Finally, it is worth providing the 2022 mean energy intensity or mean solar radiation on the case study area's Earth surface: 4.79 kWh/m2/day.

4.2. Case study building temperature and relative humidity

Considering recordings every 15 minutes, 2690 data points were collected from each sensor's log at the end of the monitoring period (1345 values for each quantity, temperature, and relative humidity). This subsection is structured as follows: indoor sensors (two devices in rooms with a different orientation) and a third sensor installed outside the building (north façade).

4.2.1. Sensors 1 and 2: indoor (south and north)

Here, temperature and relative humidity data from indoor sensors are first plotted and statistically analysed for each device separately.

Fig. 9 illustrates the behaviour of those quantities in the south bedroom (Sensor 1).

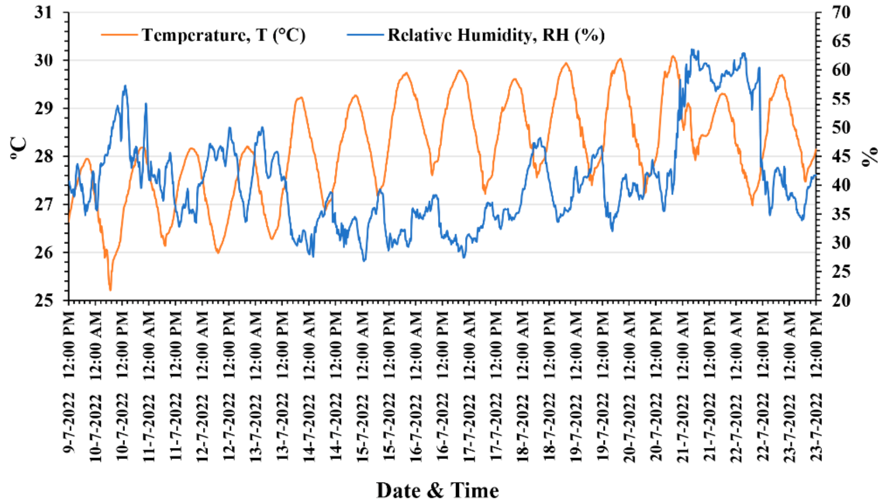

Fig. 9. Case study monitoring: Sensor 1's temperature and relative humidity. South bedroom.

Quantitative data from the previous curves are shown below (Table 2):

	Max	Min	Mean	Standard Deviation	CoV	Covariance	Correlation Coefficient
T Sensor1 (ºC)	30.09	25.21	28.18	1.03	0.04	-2.53	-0.29
RH Sensor1 (%)	63.60	26.80	40.75	8.48	0.21		

Table 2. Statistical analysis of data collected by Sensor 1. South bedroom.

The data shows what could be considered high temperature parameters for an indoor space. With windows open most of the monitoring period, the south bedroom presents an average of 2.44ºC daily difference between day and night in temperature (relative maxima and minima). There is also a greater degree of dispersion of relative humidity in contrast to indoor temperature in this sunlit room.

In terms of how the variables behave in relation to each other, covariance and correlation coefficient indicate a strong, indirect relationship between them in such a way that relative humidity markedly decreases as temperature increases, as expected, especially after noon. Relative humidity is unstable and dispersed, with values scattered across each day-night cycle. In contrast, temperature is more predictable, with more regular increases and decreases for each cycle, despite the great ordinate (y-axis) cycle breadth.

On its end, the behaviour of temperature and relative humidity of Sensor 2's data (north guest room) are displayed in Fig. 10.

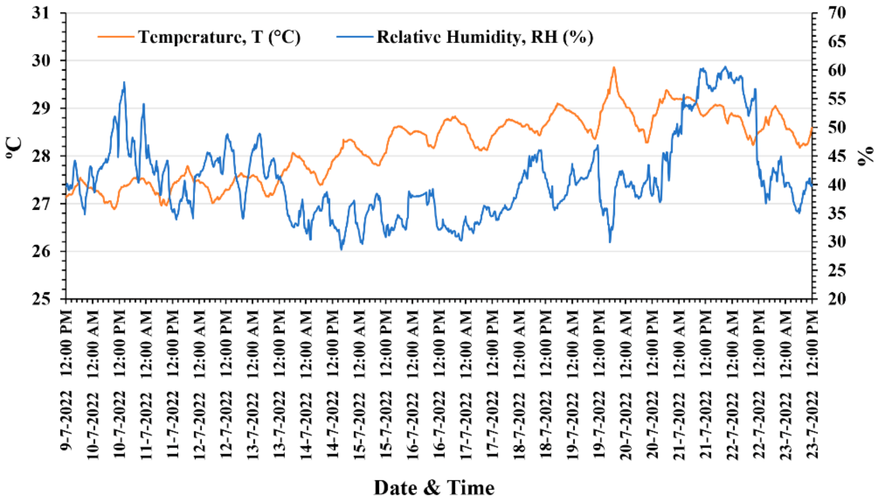

Fig. 10. Case study monitoring: Sensor 2's temperature and relative humidity. North guest room.

Table 3 gathers the statistical parameters from the above graph:

	Max	Min	Mean	Standard Deviation	CoV	Covariance	Correlation Coefficient
T Sensor2 (ºC)	29.86	26.88	28.21	0.68	0.02	0.31	0.06
RH Sensor2 (%)	60.60	28.60	40.95	7.22	0.18		

Table 3. Statistical analysis of data collected by Sensor 2. North guest room.

In comparison to Sensor 1, the north guest room experienced a more regular temperature as the data were less dispersed, both qualitatively and quantitatively, although further analysis below will show differences between their thermal behaviour. In the north guest room, the average daily temperature difference between day and night was approximately 0.81ºC. About relative humidity, records from Sensor 2 were similar on average but reached lower and higher absolute maximum and minimum values. In addition, the graph and the statistical analysis reveal an overall common behaviour of the temperature and the relative humidity.

Once data from indoor sensors have been separately displayed and analysed, it is worth presenting and studying both sources jointly in order to depict the hygrothermal performance of the case study building depending on the orientation. Prior to this, times when windows were closed because of events such as the wildfire and occupancy periods of the south bedroom are also specified (Table 4 and Table 5)—there was no occupation in the north guest room during the monitoring period.

	Date	9th July	10th July	11th July	16th July	17–18th July
Closed windows	**Room**		North		Both	South
	Time		1.00–9.45 pm		12.00–6.15 am	3.00–5.40 pm
Occupancy	**Time**	3.00–5.30 pm	1.00–10.00 am	1.00–10.00 am		11.45 pm–8.00 am
	People	1	2	1		2

Table 4. Window closing and occupancy in case study rooms.

	Date	18–19th July	20th July	21st July	22nd July	23rd July
Occupancy	**Time**	11.45 pm–8.00 am	2.00–10.30 am	1.00–10.30 am	1.30–9.30 am	1.00–8.30 am
	People	1	1	1	2	1

Table 5. Occupancy in the north guest room.

Fig. 11 shows closed windows and occupancy along with temperature values from the two sensors installed.

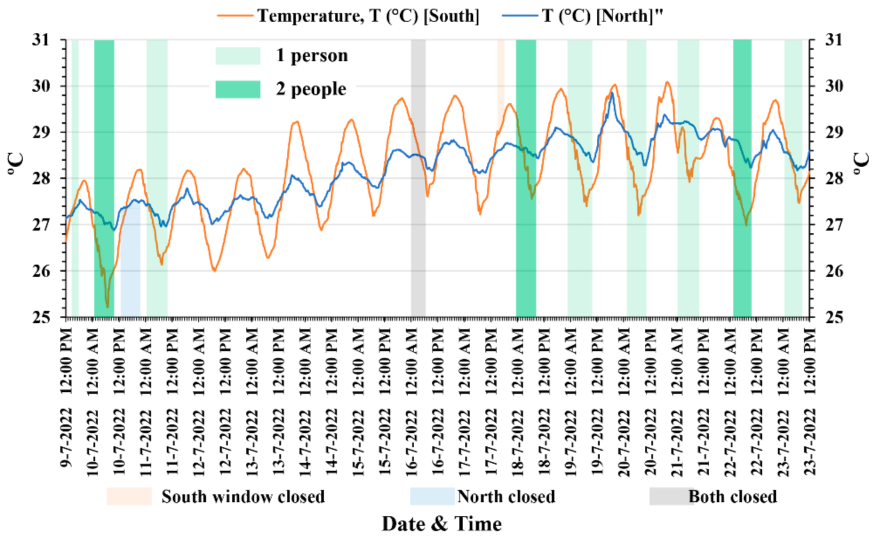

Fig. 11. Case study monitoring: Sensors 1 and 2's temperature. South bedroom and north guest room.

From the above, the situation when both windows were closed is also worth discussing. Here, temperatures decreased at night at a slower pace, particularly in the north guest room and more slightly in the south bedroom. Similarly, the routine temperature increases during sunlight followed a slower pace than usual for the two sensors (1 and 2) in cases of window closing.

For its part, Table 6 compiles the breakdown of relative maximum (daytime) and minimum (nighttime) temperature values of daily cycles during the monitoring period. This allows for the study of different room orientations in relation to each other.

Day cycle	Daily T_{max} * (South) (ºC)	Daily T_{max} (North) (ºC)	T_{max} increase (S/N)*	Daily T_{min} * (North) (ºC)	Daily T_{min} (South) (ºC)	T_{min} increase (N/S)
09/07/2022	27.95	27.54	1.01	--	--	--
10/07/2022	28.19	27.54	1.02	26.88	25.21	1.07
11/07/2022	28.17	27.79	1.01	26.96	26.14	1.03
12/07/2022	28.21	27.64	1.02	27.01	25.99	1.04
13/07/2022	29.23	28.07	1.04	27.14	26.28	1.03
14/07/2022	29.27	28.34	1.03	27.39	26.88	1.02
15/07/2022	29.74	28.62	1.04	27.80	27.19	1.02
16/07/2022	29.79	28.83	1.03	28.16	27.61	1.02
17/07/2022	29.61	28.77	1.03	28.11	27.22	1.03
18/07/2022	29.94	29.10	1.03	28.43	27.56	1.03
19/07/2022	30.03	29.86	1.01	28.35	27.40	1.03
20/07/2022	30.09	29.38	1.02	28.28	27.20	1.04
21/07/2022	29.31	29.08	1.01	28.83	27.92	1.03
22/07/2022	29.70	29.05	1.02	28.23	26.98	1.05
23/07/2022	--	--	--	28.17	27.47	1.03

*Where 'T_{max}' and 'T_{min}' account for maximum and minimum temperature, respectively, 'S' means South, and 'N' is North.

Table 6. Indoor relative maximum and minimum temperature values of day cycles.

Thus, the mean relative maximum temperature recorded by Sensor ID 1_South during the monitoring period is 2.41% higher than that deriving from the north guest room monitoring; likewise, the average relative minimum temperature from the latter sensor (Sensor ID 2_North) is circa 3.40% higher. These facts reveal that the case study building experiences slightly better indoor thermal comfort (lower temperature in summertime) in the north non-sunlit guest room during the day, as expected. In contrast, despite occupancy, the sunlit room (south) is more exposed to changes, thus seeing a more severe temperature decrease during the night, which in turn means better thermal comfort under the studied conditions of the case study.

The relative humidity recorded by both sensors was also jointly analysed (Fig. 12).

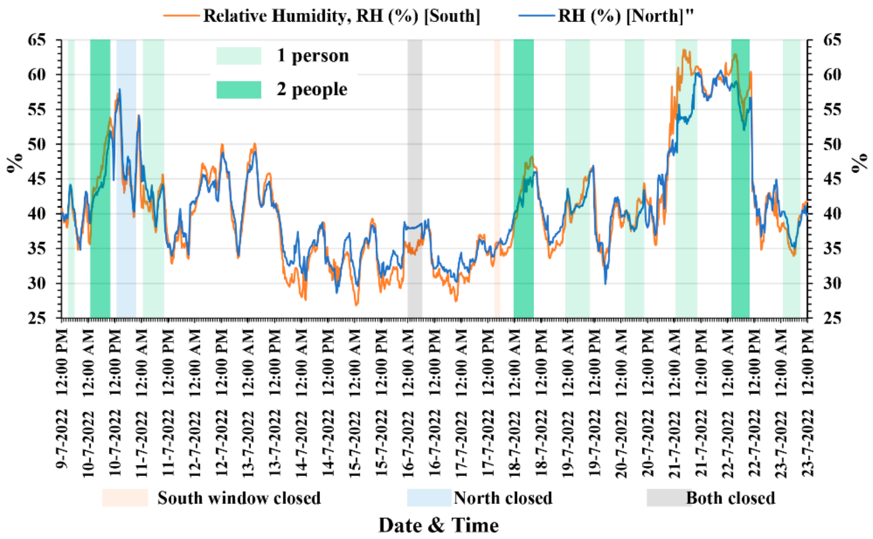

Fig. 12. Case study monitoring: Sensors 1 and 2's relative humidity. South bedroom and north guest room.

Given the complexity of relative humidity and the presence of multiple relative maximum and minimum values throughout the daily cycles, they were not calculated. Instead, the relationship between the relative humidity recorded by each sensor was quantified, obtaining a covariance of 59.59 and a correlation coefficient of 0.97.

Also supported by the graph above (Fig. 12), the statistics indicate a strong direct relationship between the data from both sensors. It is worth noting that occupancy makes the south bedroom's relative humidity higher at night since the north guest room is generally superior the rest of the time.

4.2.2. Sensor 3: outdoor (north façade)

This subsection includes the analysis of i) the case study's outdoor ambient conditions, studying data recorded by Sensor ID 3_Exterior and relevant meteorological parameters deriving from MERRA-2, and ii) the behaviour of Sensor ID's 1_South and 2_North against 3_Exterior in order to characterise the building performance.

Firstly, given that temperature and relative humidity values from the building monitoring were recorded every 15 minutes, in contrast to the hourly recording for wind speed at 10 m (MERRA-2 data), values corresponding to the 15, 30, and 45 minutes between hours were linearly interpolated to complete the satellite data. As a result, the joint analysis of the variables is straightforward, with a wind speed value for every temperature and relative humidity datum (Fig. 13).

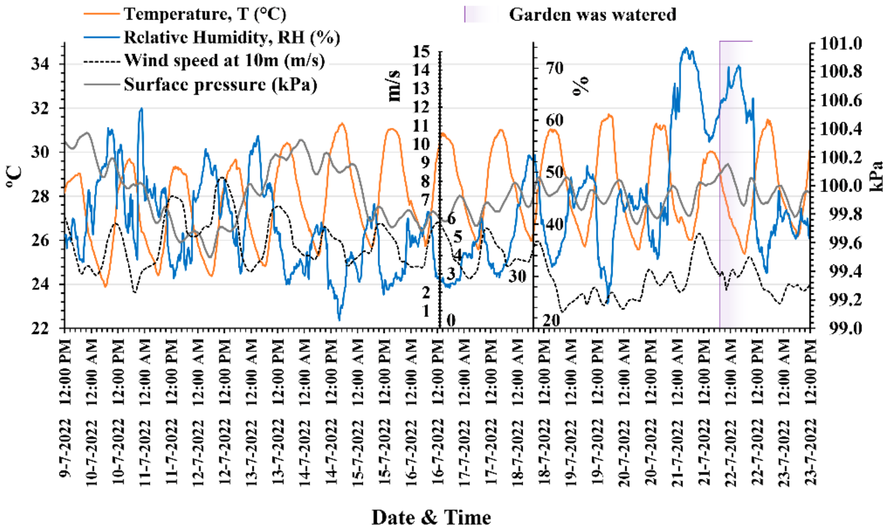

Fig. 13. Case study monitoring: outdoor ambient temperature and relative humidity, wind speed and surface pressure. Source: sensor ID 3_Exterior and NASA's (1981) 'POWER Project' Data Access Viewer, respectively.

As previously seen, Table 7 gathers statistical parameters to contrast quantities recorded by a sensor installed in the case study building and, this time, satellite meteorological data.

	Max	Min	Mean	Standard Deviation	CoV	Covariance	Correlation Coefficient
T Sensor3 (ºC)	31.62	24.00	28.05	1.94	0.07	-11.30	-0.53
RH Sensor3 (%)	73.90	22.70	42.18	11.06	0.26		
Surface Pressure (kPa)	100.32	99.50	99.92	0.16	0.00		
				SurPress* against T Sensor3		-0.03	-0.10
				SurPress against RH Sensor3		0.40	0.22
				SurPress against WS10*		0.01	0.04
Wind Speed at 10 m (m/s)	8.16	0.89	3.80	1.57	0.41		
				WS10 against T Sensor3		0.00	0.00
				WS10 against RH Sensor3		-2.40	-0.14

*Where 'SurPress' accounts for surface pressure and 'WS10' for wind speed at 10 m.

Table 7. Statistical analysis of sensor temperature and relative humidity data against meteorological data. Source: own data and NASA's (1981) 'POWER Project' Data Access Viewer, respectively.

The surface pressure remains predominantly stable throughout the monitoring period. In view of Fig. 13, the 12-hour cycles of surface pressure correspond to fluctuations in relative humidity, whereas temperature exhibits cycles of approximately 24h. Surface pressure rises and falls rapidly alongside temperature, coinciding with the onset and conclusion of each temperature cycle. However, two cycles of surface pressure occur during the solar radiation cycle, at approximately the highest temperature value, making the surface pressure reach a lower value.

Regarding the behaviour of quantities between each other, it is worth highlighting the accordance of outdoor temperature with wind speed and surface pressure. In contrast, relative humidity is significantly influenced, especially by wind speed, to a greater extent. It has an indirect relationship with wind speed and a direct, albeit lesser, connection with surface pressure.

Secondly, outdoor sensor data were compared to those from Sensors 1_South and 2_North so that the building's hygrothermal behaviour could be depicted (Fig. 14).

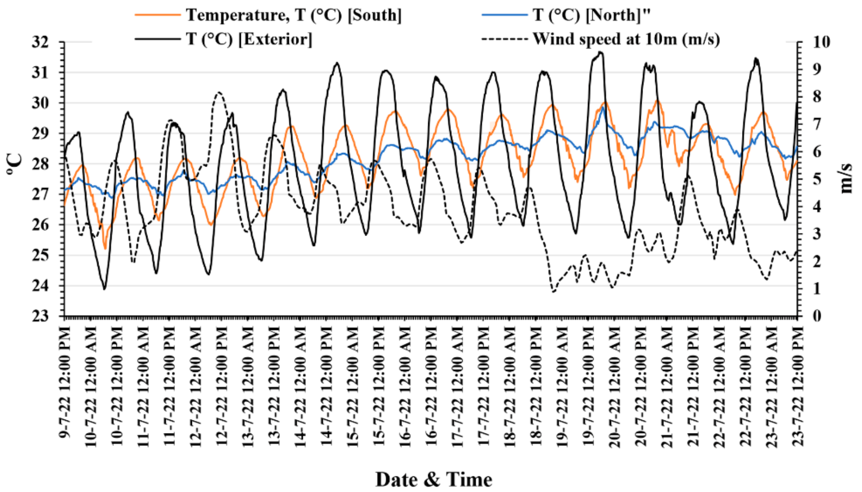

Fig 14. Case study monitoring: indoor and outdoor ambient temperature and wind speed. Source: sensors 1, 2, and 3, and NASA's (1981) 'POWER Project' Data Access Viewer, respectively.

In the graph above, the vertical scale remained constant to facilitate the identification of extreme values from each of the three temperature data sources.

For its part, Table 8 quantifies the relationship between indoor and outdoor temperature values from each sensor.

	T Sensor 3 vs 1	T Sensor 3 vs 2
Covariance	1.30	0.58
Correlation Coefficient	0.65	0.44

Table 8. Statistical analysis of temperature data collected by all sensors.

Table 9 indicates a more direct and stronger relationship between outdoor temperature and that from the south bedroom, which is more extreme than the temperature from Sensor 2.

Day cycle	Daily T_{max} (Exterior) (ºC)	Daily T_{max} (South) (ºC)	T_{max} increase (Ext/S)	Daily T_{min} (North) (ºC)	Daily T_{min} (Exterior) (ºC)	T_{min} increase (N/Ext)
09/07/2022	29.04	27.95	1.04	--	--	--
10/07/2022	29.70	28.19	1.05	26.88	23.88	1.13
11/07/2022	29.35	28.17	1.04	26.96	24.41	1.10
12/07/2022	29.67	28.21	1.05	27.01	24.37	1.11
13/07/2022	30.44	29.23	1.04	27.14	24.82	1.09
14/07/2022	31.32	29.27	1.07	27.39	25.32	1.08
15/07/2022	31.06	29.74	1.04	27.80	25.67	1.08
16/07/2022	30.87	29.79	1.04	28.16	25.73	1.09
17/07/2022	31.01	29.61	1.05	28.11	25.58	1.10
18/07/2022	31.04	29.94	1.04	28.43	25.97	1.09
19/07/2022	31.72	30.03	1.06	28.35	25.71	1.10
20/07/2022	31.31	30.09	1.04	28.28	25.58	1.11
21/07/2022	30.04	29.31	1.02	28.83	26.00	1.11
22/07/2022	31.47	29.70	1.06	28.23	25.37	1.11
23/07/2022	--	--	--	28.17	26.16	1.08

*Where 'T_{max}' and 'T_{min}' account for maximum and minimum temperature, respectively, 'S' means South, 'N' is North and 'Ext' is exterior.

Table 9. Indoor and outdoor relative maximum and minimum temperature values of day cycles.

In addition, relative maximum and minimum temperature values of daily cycles were also calculated (Table 9); this time, the most unfavourable scenarios were addressed, such as the maximum indoor temperature values, both daytime and nighttime, as they affect thermal comfort. The maximum temperature of the 23rd of July and the minimum of the 9th were not calculated as those days were not fully monitored.

Given the results above, the average relative maximum outdoor daytime temperature is 4.6% higher than that recorded by Sensor 1 in the south bedroom, which, in turn, represents a mean difference of approximately 1.36ºC. In contrast, the non-sunlit north guest room shows an average relative minimum indoor temperature of around 10% higher than the exterior at night, reaching a mean difference of 2.55ºC, which, by itself, may entail thermal discomfort inside the building under those conditions.

Besides, the typical temperature drop in the late afternoon, particularly in the south-facing room—it is the most exposed to solar radiation—occurs with a delay of approximately 2 to 4 hours compared to the exterior. This may be due to the thermal inertia effects of the building envelope still applying during this period, as it absorbs energy throughout the day. In contrast, due to the thermal envelope's characteristics and as a result of solar activity since sunrise, the temperature increase in the building takes between 1 and 2 hours in comparison to the outside.

Regarding the wind, Table 10 gathers statistical parameters of its relationship with sensor temperature data.

	WS vs T Sensor1	WS vs T Sensor2	WS vs T Sensor3
Covariance	-0.78	-0.64	0.00
Correlation Coefficient	-0.49	-0.61	0.00

Table 10. Statistical analysis of wind speed–temperature data gathered and collected by all sensors, respectively.

These data show the opposite behaviour of wind against indoor temperatures, as they generally increase when wind speed decreases. What is more, the unstable, non-uniform curves of temperatures correspond to periods with irregular wind speeds, with drops and rises of a different ordinate (*y*-axis) cycle breadth. This could indicate that wind speed affects indoor temperature behaviour and partly the outdoor temperature while sharing an overall common trend with the latter.

With respect to relative humidity, this research revealed its complexity both inside and outside the building. For the first time in this chapter, relative humidity data from sensors 1, 2, and 3 are displayed together so that their complex behaviour is depicted (Fig. 15). Again, the scale of the vertical axis remains constant.

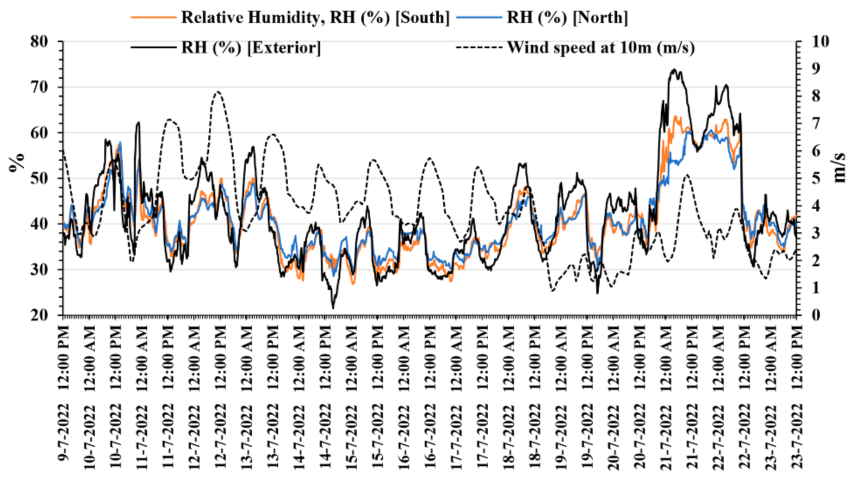

Fig. 15. Case study monitoring: indoor and outdoor ambient relative humidity and wind speed. Source: sensors 1, 2, and 3, and NASA's (1981) 'POWER Project' Data Access Viewer, respectively.

Statistical data is also provided in Table 11 below:

	RH Sensor 3 vs 1	RH Sensor 3 vs 2
Covariance	87.51	72.76
Correlation Coefficient	0.94	0.91

Table 11. Statistical analysis of relative humidity data collected by all sensors.

Therefore, it is patent that both indoor relative humidities behave in accordance with outdoor data, with a higher correspondence of data recorded by Sensor 1_South, a room that is more exposed to the exterior.

Finally, in terms of wind activity, as seen in Fig. 15, its relationship with relative humidity data from all sources (sensors) becomes more intricate. Table 12 statistically analyses their connection.

	WS vs RH Sensor 1	WS vs RH Sensor 2	WS vs RH Sensor 3
Covariance	-0.62	-0.79	-2.40
Correlation Coefficient	-0.05	-0.07	-0.14

Table 12. Statistical analysis of MERRA-2 wind speed and relative humidity data collected by all sensors.

While indoor relative humidity data follow a slightly different distribution in comparison with wind speed, outdoor data from Sensor ID 3_Exterior is clearly against its behaviour, showing an indirect relationship that may imply relative humidity drops as the wind increases.

5. Conclusions

The adaptation of building occupants to unfavourable outdoor environmental conditions resides in two primary aspects: the passive strategies implemented in the building, comprising design features and subject to construction quality, and strategies of use, such as the control of window openings, sun protection solutions, among others inherent to their behaviour.

As far as the authors of this chapter know, this is the first time the hygrothermal performance of a building has been analysed under a series of unfavourable conditions affecting both indoor and outdoor ambient. In particular, considering the Mediterranean climate in summer, these conditions consisted of i) keeping windows open during a high-temperature season and ii) a nearby wildfire, which had a clear effect on the area's moisture index and could have impacted recorded relative humidity.

The case study building was monitored for two weeks in July 2022 in three key locations using temperature and relative humidity sensors (Sensor 1_South, 2_North, and Sensor ID 3_Exterior). The results indicated that the case study building's thermal inertia made it retain heat for 2 to 4 hours from the logical temperature drop at night, with the most exposed room (south bedroom) reaching an average 4.40% reduction in temperature in relation to the mean maximum outdoor temperature; likewise, the indoor temperature rise took from 1 to 2 hours to occur during sun activity from early morning. The non-sunlit north guest room showed a 10% higher average relative minimum daily indoor temperature (circa 28ºC) in comparison with the outside, thus revealing worse thermal behaviour (greater thermal discomfort) than the south bedroom at night. In addition, window closing had an impact on both indoor temperature and relative humidity inasmuch as their rises and drops happened at a slower pace, as expected. Similarly, their values increased as wind speed decreased, the latter following cycles of 12 hours against the daily cycles (24 hours) of temperature and humidity. For its part, building occupation in the south bedroom caused relative humidity to be slightly higher than that of the north guest room. However, the less exposed room (north) presents higher relative humidity despite the lack of occupation. In this sense, having installed sensor 3 also on the north façade, it was not possible to evaluate the effect of watering the garden on the case study's indoor hygrothermal conditions.

All considered, future work would involve researching the role of indoor air velocity in temperature and relative humidity changes. Similarly, the impact of closing the window of the south bedroom during the day (the most affected room at a critical moment) on the building's hygrothermal behaviour is yet to be explored.

Acknowledgements

This work has been supported by funding for a post-doctoral researcher contract from the VI Plan Propio de Investigación y Transferencia of Universidad de Sevilla (reference VIPPIT-2020-II.5), Spain.

This work has also been funded by the England European Regional Development Fund (ERDF) (reference 08R20S04177) as part of the European Structural and Investment Funds Growth Programme 2014-2020, the University of Nottingham, and Nottingham Trent University through the 'Live Experiential and Digital Diversification – Nottingham' (LEADD:NG) project.

The authors also wish to thank the Product Innovation Centre at the School of Architecture, Design and the Built Environment, Nottingham Trent University, for access to their sensors.

Finally, as stated in this chapter, third-party satellite data were obtained from the NASA Langley Research Center (LaRC) POWER Project, which is funded through the NASA Earth Science/Applied Science Program.

References

Acaire (2022) Seguimiento del incendio de la Sierra de Mijas de julio de 2022. In: Incend. en la Costa del Sol Sierra Mijas. https://www.acaire.es/2022/07/18/seguimiento-incendio-sierra-mijas-julio-2022/. Accessed 10 Nov 2023

Antón D, Amaro-Mellado J-L (2021) Engineering Graphics for Thermal Assessment: 3D Thermal Data Visualisation Based on Infrared Thermography, GIS and 3D Point Cloud Processing Software. Symmetry (Basel) 13:335. https://doi.org/10.3390/sym13020335

Antón D, Carretero-Ayuso MJ, Moyano-Campos J, Nieto-Julián JE (2022) Laser Scanning Intensity Fingerprint: 3D Visualisation and Analysis of Building Surface Deficiencies. In: Bienvenido-Huertas D, Moyano-Campos J (eds) New Technologies in Building and Construction. Springer Nature Singapore, Singapore, pp 207–223

Arsad FS, Hod R, Ahmad N, et al (2023) Assessment of indoor thermal comfort temperature and related behavioural adaptations: a systematic review. Environ Sci Pollut Res 30:73137–73149. https://doi.org/10.1007/s11356-023-27089-9

Balali A, Yunusa-Kaltungo A, Edwards R (2023) A systematic review of passive energy consumption optimisation strategy selection for buildings through multiple criteria decision-making techniques. Renew Sustain Energy Rev 171:113013. https://doi.org/10.1016/j.rser.2022.113013

Borghero L, Clèries E, Péan T, et al (2023) Comparing cooling strategies to assess thermal comfort resilience of residential buildings in Barcelona for present and future heatwaves. Build Environ 231:110043. https://doi.org/10.1016/j.buildenv.2023.110043

Chvatal KMS, Corvacho H (2009) The impact of increasing the building envelope insulation upon the risk of overheating in summer and an increased energy consumption. J Build Perform Simul 2:267–282. https://doi.org/10.1080/19401490903095865

Daghigh R (2015) Assessing the thermal comfort and ventilation in Malaysia and the surrounding regions. Renew Sustain Energy Rev 48:681–691. https://doi.org/10.1016/j.rser.2015.04.017

Dirección General de Política Forestal y Biodiversidad (2023) Resolución de la dirección general de política forestal y biodiversidad por la que se aprueba el plan integrado de caza de los terrenos afectados por el incendio de Mijas en el año 2022. Consejería de Sostenibilidad, Medio Ambiente y Economía Azul (Junta de Andalucía)

Dirección General de Protección Civil y Emergencias (2023) Informe de incendios forestales 2022

European Space Agency (ESA), T-Systems (2017) Copernicus Browser. In: Copernicus Data Sp. Ecosyst. https://dataspace.copernicus.eu/browser/. Accessed 10 Nov 2023

Google Inc. (2023) Google Earth Pro

Instituto de Estadística y Cartografía de Andalucía (2023) Alhaurín de la Torre. In: Andalucía pueblo a pueblo - Fichas Munic. https://www.juntadeandalucia.es/institutodeestadisticaycartografia/sima/ficha.htm?mun=29007. Accessed 10 Nov 2023

Kim A, Wang S, Kim J-E, Reed D (2019) Indoor/Outdoor Environmental Parameters and Window-Opening Behavior: A Structural Equation Modeling Analysis. Buildings 9:94. https://doi.org/10.3390/buildings9040094

Lai D, Jia S, Qi Y, Liu J (2018) Window-opening behavior in Chinese residential buildings across different climate zones. Build Environ 142:234–243. https://doi.org/10.1016/j.buildenv.2018.06.030

Li N, Li J, Fan R, Jia H (2015) Probability of occupant operation of windows during transition seasons in office buildings. Renew Energy 73:84–91. https://doi.org/10.1016/j.renene.2014.05.065

Ministerio de Vivienda (2006) Real Decreto 314/2006, de 17 de marzo, por el que se aprueba el Código Técnico de la Edificación. Boletín Oficial del Estado, Spain

Mochida A, Yoshino H, Takeda T, et al (2005) Methods for controlling airflow in and around a building under cross-ventilation to improve indoor thermal comfort. J Wind Eng Ind Aerodyn 93:437–449. https://doi.org/10.1016/j.jweia.2005.02.003

NASA (1981) POWER Data Access Viewer. In: Predict. Worldw. Energy Resour. https://power.larc.nasa.gov/data-access-viewer/. Accessed 10 Nov 2023

NASA (2020) POWER Data Methodology. In: NASA POWER. https://power.larc.nasa.gov/docs/methodology/. Accessed 10 Nov 2023

Tamaskani Esfahankalateh A, Farrokhzad M, Saberi O, Ghaffarianhoseini A (2021) Achieving wind comfort through window design in residential buildings in cold climates, a case study in Tabriz city. Int J Low-Carbon Technol 16:502–517. https://doi.org/10.1093/ijlct/ctaa082

Zaki WRM, Nawawi AH, Sh.Ahmad S (2012) Environmental Prospective of Passive Architecture Design Strategies in Terrace Houses. Procedia - Soc Behav Sci 42:300–310. https://doi.org/10.1016/j.sbspro.2012.04.194